INL/CON-22-65883-Revision-0

On Practical Aspects of Variational Consistency in Contact Dynamics

May 2023

Changing the World's Energy Future

Antonio Martin Recuero, Alexander D Lindsay

Idaho National Laboratory

INL/CON-22-65883-Revision-0

On Practical Aspects of Variational Consistency in Contact Dynamics

Antonio Martin Recuero, Alexander D Lindsay

May 2023

Idaho National Laboratory
Idaho Falls, Idaho 83415

http://www.inl.gov

Prepared for the
U.S. Department of Energy
Under DOE Idaho Operations Office
Contract DE-AC07-05ID14517

On practical aspects of variational consistency in contact dynamics

Antonio Recuero*

Idaho National Laboratory
Computational Mechanics and Materials Department
Idaho Falls, Idaho 83415
Email: antonio.martinrecuero@inl.gov

Alexander Lindsay

Idaho National Laboratory
Computational Frameworks Department
Idaho Falls, Idaho 83415
Email: alexander.lindsay@inl.gov

Usage of contact mechanics methodologies is a pervasive modeling requirement in dynamic simulations. While for some trivial problems, solutions taken from analytical geometry are available, use of a finite element framework is common to achieve formulation generality. This work explores two dynamic contact formulations: one based on the traditional node-to-segment (NTS) approach, and a variationally consistent segment-to-segment (STS) mortar formulation. The NTS formulation employed here enforces the constraints kinematically (i.e., the interpenetration is enforced to the solver tolerance), whereas the mortar approach uses Lagrange multipliers to enforce the contact constraints. Both approaches are implemented in the open-source finite element framework Multiphysics Object-Oriented Simulation Environment (MOOSE). The results highlight two relevant contact-interface-related dynamic phenomena in finite element simulations. First, stabilization of contact constraints is discussed, taking into account the evolution of the total energy in a benchmark problem. Second, the influence of finite element discretization on both of the aforementioned contact formulations is analyzed by exercising a large-deformation example with continuous relative sliding. Variationally consistent contact approaches such as the mortar formulation lead to improved energy preservation and avoid spurious excitation of the system's frequencies. This is especially relevant in settings where inertia and vibrations are of importance.

*Corresponding author.

1 INTRODUCTION

Contact formulations and their corresponding algorithms are commonplace in simulations of multibody and nonlinear systems, for which consideration of inertia is key. For the computational modeling of systems of industrial relevance, general discretization techniques are often required. In this research area, contact mechanics algorithms applicable to the finite element method have been extensively investigated, and a large body of related literature is available (e.g., see textbooks [1, 2]). Enforcement of the mechanical interaction of domain boundaries is typically performed in finite element multibody system applications by using a node-to-segment (NTS) approach. This choice usually leads to relatively simple algorithms whose main feature is the matching of a node—typically on a secondary surface—to an opposing, primary surface by using some criterion, such as the closest point projection algorithm.

Other finite element contact approaches employ variationally consistent formulations to tackle the contact problem on non-matching discretized interfaces. Instances of this are the mortar formulation [3, 4, 5], Nitsche's formulation [6], and the local average contact method [7, 8]. As an example, the consistency of the mortar finite element discretization ultimately relies on the constraint enforcement on segments on a lower-dimensional domain with proper Lagrange multiplier spaces [4]; avoidance of locking effects and unphysical oscillations, and passing the contact patch test are proof of such consistency. The lower-dimensional segments are built upon each numerical evaluation. That is, the non-interpenetration, frictional nonlinear complementarity conditions and their residuals (or contact forces) are computed on a lower-dimensional domain [9]. For example, for a 2-D problem, the constraints are enforced on a discretized 1-D domain built via a projection procedure that accounts for both discretized boundaries.

Use of a consistent variational formulation for modeling contact interaction offers known practical benefits. First, such formulations (e.g., the mortar formulation) exhibit optimal convergence rates with mesh refinement (see [10]) and pass the contact patch test [11]. Additionally, the smoothness of the solution guarantees heightened accuracy because, unlike with an NTS approach, there are no formulation-driven discrete events, as contacting surfaces slide relatively to each other. In other words, sudden nodal contacts do not suddenly appear and disappear as the simulation progresses. Finally, the use of consistent formulations has a clear effect on numerical convergence. Regardless of whether the system solved includes inertia, the potential consistency of a segment-to-segment (STS) approach helps solve tough, highly nonlinear problems and enables these problems to converge to tighter tolerances.

Mortar contact formulations have been applied to nonlinear dynamic problems [12] and can potentially be extended to formulations developed within the multibody system community, such as the finite element floating frame of reference formulation [13]. Indeed, requirements pertaining to element type and interpolation order are consistent with those of the linear finite element formulations used to capture small deformation from a floating frame.

In this work, we use a mortar formulation developed in the open-source software Multiphysics Object-Oriented Simulation Environment MOOSE [14], whose general mortar segment generation capability allows for the application of mortar approaches to various problems, including continuity, thermal, and mechanical contact physics. The Lagrange multipliers for the contact problem use dual basis interpolation [5], and the constraint equations for normal and frictional contact are of the form presented in [15]. An extension of this dual mortar approach to dynamic simulations is provided in [16]. For the current paper, this general dual mortar approach is employed, albeit with small differences described in later sections. The NTS approach is also briefly described, but mostly aligns with the existing approaches described in the literature (e.g., [17]). The formulations, numerical results, and discussion presented in this manuscript focus on kinematic or exact enforcement of the mechanical contact constraint. In other words, the penalty approach, by which constraints are not satisfied to solver tolerances, is not considered herein.

This work aims to provide new insight into the use of contact formulations in a dynamic setting by performing a practical comparison between (1) a typical NTS formulation and (2) a general mortar contact formulation recently implemented natively in MOOSE, providing flexibility in the selection of finite element orders, mesh geometry, and interpolation functions. The present work first outlines and leverages MOOSE's native implementation of a finite element mechanical mortar framework for dynamic applications. To solve the contact constraints, automatic differentiation is used, thus enabling quicker development turnaround times.

While there is extensive literature on both the NTS and STS approaches to contact mechanics, in the present paper, we intend to provide numerical results that clearly argue the importance of variational consistency in the formulation of contact dynamics. To that effect, the evolution of the system's elastic/kinetic energies and contact forces, along with the excitation of the system's fundamental frequencies, are analyzed in the Numerical Results section.

The paper is structured as follows: the fundamental equations of solid mechanics, including contact interaction, are discussed in Section 2. Sections 3 and 4 briefly describe the STS and NTS formulations used in the Numerical Results section. While the NTS formulation has long existed in MOOSE, this manuscript represents the first time that development of the STS approach for dynamic applications has been presented. Section 5 shows numerical results highlighting the importance of contact constraint stability and mortar formulation smoothness for benchmark dynamic problems. This section highlights the fact that variational consistency can be key to successfully simulating challenging contact dynamics problems. Finally, Section 6 presents a discussion on the obtained numerical results.

2 CONTACT MECHANICS EQUATIONS

Here, we present the fundamental equations for mechanical contact enforcement, which were used to generate the numerical results. Assuming two bodies that come into mechanical contact, we define the domains $\Omega^{(\gamma)}$, $\gamma \in \{1, 2\}$. The potential contact surface is denoted by $\Gamma_c^{(\gamma)}$, which is a lower-dimensional subset on the boundary $\partial\Omega^{(\gamma)}$.

The differential equations describing the conservation of momentum equation are solved for all system domains $\Omega^{(\gamma)}$. The equations then take the following form:

$$\begin{aligned} \nabla \cdot \boldsymbol{\sigma}^{(\gamma)} + \boldsymbol{b}^{(\gamma)} &= \rho \ddot{\boldsymbol{u}}^{(\gamma)} \quad \text{in } \Omega^{(\gamma)}, \\ \boldsymbol{u}^{(\gamma)} &= \bar{\boldsymbol{u}}^{(\gamma)} \quad \text{on } \Gamma_u^{(\gamma)}, \\ \boldsymbol{\sigma}^{(\gamma)} \cdot \boldsymbol{n}_t^{(\gamma)} &= \bar{\boldsymbol{t}}^{(\gamma)} \quad \text{on } \Gamma_t^{(\gamma)}, \end{aligned} \tag{1}$$

where $\boldsymbol{\sigma}^{(\gamma)}$ is the Cauchy stress tensor, $\boldsymbol{u}^{(\gamma)}$ is the displacement vector, $\boldsymbol{b}^{(\gamma)}$ is the body force, ρ is density, $\ddot{\boldsymbol{u}}^{(\gamma)}$ is the vector of accelerations, $\boldsymbol{n}_t^{(\gamma)}$ is the unit normal to the traction boundary, $\bar{\boldsymbol{u}}^{(\gamma)}$ is the prescribed displacement boundary condition, and $\bar{\boldsymbol{t}}^{(\gamma)}$ is the prescribed traction boundary condition. The displacement, traction, and contact boundaries are assumed to be disjoint (i.e., $\Gamma_u^{(\gamma)} \cap \Gamma_t^{(\gamma)} = \Gamma_t^{(\gamma)} \cap \Gamma_c^{(\gamma)} = \Gamma_u^{(\gamma)} \cap \Gamma_c^{(\gamma)} = \emptyset$).

The following mechanical normal contact constraints are defined on $\Gamma_c^{(1)}$:

$$g_n \geq 0, \;\; p_n \leq 0, \;\; p_n g_n = 0, \tag{2}$$

where g_n is the gap function that measures the distance between the two bodies and p_n is the normal contact pressure. This gap distance can be defined for a point on the secondary surface (superscript (1)) with respect to the primary surface (superscript (2)) as:

$$g_n = -\boldsymbol{n}^{(1)} \cdot \left(\boldsymbol{x}^{(1)} - \mathcal{P}\boldsymbol{x}^{(2)}\right), \tag{3}$$

where $\mathcal{P}$ represents a projection of variables from the primary side to the secondary side, and $\boldsymbol{n}^{(1)}$ denotes the outward unit normal on the secondary surface. Equation 3 defines general Hertz-Signorini-Moreau contact conditions. Frictional constraints of the Coulomb type may be expressed as follows:

$$\begin{aligned} &\Phi := ||\boldsymbol{t}_\tau|| - \mu|p_n| \leq 0, \\ &\boldsymbol{v}_{\tau,\mathrm{rel}} + \beta \boldsymbol{t}_\tau = \boldsymbol{0}, \;\; \beta \geq 0, \;\; \Phi\beta = 0, \end{aligned} \tag{4}$$

where $\boldsymbol{t}_\tau$ is the tangential contact force, μ is the coefficient of friction, $\boldsymbol{v}_{\tau,\mathrm{rel}}$ is the relative tangential velocity, and β is a variable that relates the relative sliding velocity to the tangential force, thereby defining stick and slip states. The overall contact traction is then the sum of the normal and tangential contributions: $\boldsymbol{t}_c^{(1)} = p_n \boldsymbol{n}^{(1)} + \boldsymbol{t}_\tau$. Note that in our implementation, the discretized secondary side $\Gamma_c^{(1)}$ determines the interpolation of normal and tangent vectors used for enforcing the contact constraints and the computation of the residual vector (i.e., the contact forces). The approach used herein is therefore biased; i.e. different continuity results are obtained if the role of contacting surfaces (i.e. "primary" and "secondary") is swapped. Typically, we select the more finely discretized contacting surface as "secondary". Such a choice leads to more accurate constraint enforcement and reduces the contact constraint dependencies on primary surface's displacement variables. Non-biased approaches to mortar contact exist in the literature [18].

The balance of the linear momentum is enforced by introducing a Lagrange multiplier vector $\boldsymbol{\lambda}$. Both normal and tangential contact contributions are considered. $\boldsymbol{\lambda} = -\boldsymbol{t}_c^{(1)}$, meaning that the total Lagrange multiplier vector represents the negative contact traction on the secondary side. The variational equations for the mechanical problem may be expressed as:

$$\begin{aligned} &\sum_{\gamma=1}^{2} \left\{ \int_{\Omega^{(\gamma)}} \left(\delta \boldsymbol{\varepsilon}^{(\gamma)} : \boldsymbol{\sigma}^{(\gamma)}\right) \, \mathrm{d}\Omega - \int_{\Omega^{(\gamma)}} \boldsymbol{b}^{(\gamma)} \cdot \delta \boldsymbol{u}^{(\gamma)} \, \mathrm{d}\Omega \right. \\ &\quad \left. - \int_{\Gamma_t^{(\gamma)}} \left(\bar{\boldsymbol{t}}^{(\gamma)} \cdot \delta \boldsymbol{u}^{(\gamma)}\right) \, \mathrm{d}s \right\} \\ &\quad + \int_{\Gamma_c^{(1)}} \boldsymbol{\lambda} \left(\delta \boldsymbol{u}^{(1)} - \mathcal{P} \delta \boldsymbol{u}^{(2)}\right) \, \mathrm{d}s = \\ &\quad \sum_{\gamma=1}^{2} \int_{\Omega^{(\gamma)}} \left(\rho^{(\gamma)} \ddot{\boldsymbol{u}}^{(\gamma)} \cdot \delta \boldsymbol{u}^{(\gamma)}\right) \, \mathrm{d}\Omega, \end{aligned} \tag{5}$$

where $\boldsymbol{\varepsilon}^{(\gamma)} = \left(\nabla \boldsymbol{u}^{(\gamma)} + \nabla \boldsymbol{u}^{(\gamma)\intercal}\right)/2$ is the linearized version of the Green-Lagrange strain tensor, which is utilized in the updated Lagrangian approach to model finite strain deformation, and δ denotes the variational operator. A strongly objective finite strain incremental strategy is employed together with the updated Lagrangian formulation [19].

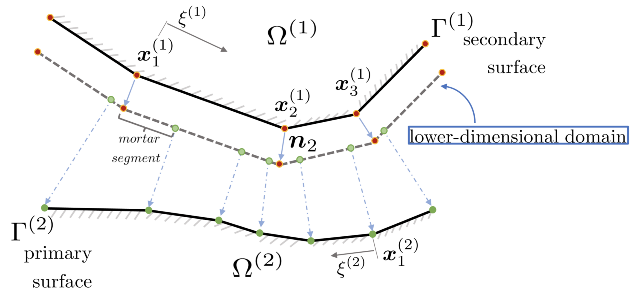

Fig. 1: SCHEME SHOWING DISCRETIZATION OF THE LOWER-DIMENSIONAL MESH WHERE CONTACT CONSTRAINTS ARE ENFORCED. RESIDUALS AND LAGRANGE MULTIPLIERS ARE THEN COMPUTED ON THE SECONDARY SURFACE (1).

3 DISCRETIZED MORTAR MECHANICAL CONTACT EQUATIONS

The approach used in this work relies on the dual interpolation of Lagrange multipliers (e.g. normal contact pressure or frictional contact pressure). The dual approach offers several advantages when employed for mortar contact. First, the variable coupling through the mortar segment mesh (Fig. 1) is made localized, and the first mortar matrix becomes diagonal. In addition, the contact conditions become pointwise, allowing for both a straightforward interpenetration in a classical way and the use of contact active set strategies (see [20] for more details). Thus, this work employs a dual mortar approach.

We provide the discretized contact constraints, skipping intermediate functional analysis derivations. These constraints are included in the solution of the entire system of equations, and may be solved via a semi-smooth Newton or a Jacobian-free Newton-Krylov approach [21]. This primal-dual active set strategy [22] employs dual shape functions for the interpolation of mechanical contact Lagrange multipliers.

For normal contact constraints, the discretized equations particularized at a node j, $\boldsymbol{C}_j$, may be written as:

$$\boldsymbol{C}_j(\boldsymbol{u}, \boldsymbol{\lambda}) = \lambda_{n,j} - \max(0, \lambda_{n,j} - c_n \tilde{g}_{n,j}) = 0, \quad c_n > 0, \tag{6}$$

where $\lambda_{n,j}$ is the normal contact Lagrange multiplier (whose physical meaning is contact pressure) at node j, $\tilde{g}_{n,j}$ is a gap distance computed in the mortar sense at node j (see [4]), and c_n is a numerical parameter whose value is selected to improve convergence behavior without affecting the numerical results. Unlike with NTS, the weighted gap distance is computed in a manner that accounts for the contribution of nearby mortar segments via numerical integration. This idea can be mathematically expressed as:

$$\tilde{g}_{n,j} = \int_{\gamma_c^{(1)}} \phi_j(\boldsymbol{\xi}) g^h(\boldsymbol{\xi}) \mathrm{d}\gamma_c^{(1)}, \tag{7}$$

where $\gamma_c^{(1)}$ represents the current configuration of the secondary surface $\Gamma^{(1)}$, ϕ_j denotes the Lagrange multiplier interpolation function at node j, and $\boldsymbol{\xi}$ is the parametric coordinate vector, which takes quadrature point values for a full numerical integration. The quantity g^h refers to a pointwise evaluation of the normal gap, in accordance with the appropriate integration rule.

For its frictional counterpart, the contact equations, $\boldsymbol{T}_j$, include a primal-dual active set strategy that iteratively separates nodes into contact/no-contact and stick/slip conditions:

$$\begin{aligned}
&\boldsymbol{T}_j(\boldsymbol{u}, \boldsymbol{\lambda}) = \max(\mu(\lambda_{n,j} - c_n \tilde{g}_{n,j}), \|\boldsymbol{\lambda}_{t,j} + c_t \tilde{\boldsymbol{v}}_{t,rel,j}\|)\boldsymbol{\lambda}_{t,j} \\
&- \mu \max(0, \lambda_{n,j} - c_n \tilde{g}_{n,j}) \cdot (\boldsymbol{\lambda}_{t,j} + c_t \tilde{\boldsymbol{v}}_{t,rel,j}) = \boldsymbol{0}, \\
&c_n, c_t > 0,
\end{aligned} \tag{8}$$

where $\boldsymbol{\lambda}_{t,j}$ refers to node j's frictional Lagrange multipliers, $\tilde{\boldsymbol{v}}_{t,rel,j}$ is the relative tangential velocity computed on the lower-dimensional mortar segment mesh (analogously to Eqn. 7), and c_t is a numerical parameter whose sole purpose is to improve convergence. Satisfactory selection of c_n and c_t is typically linked to the mechanical properties of the bodies in contact with each other. All that is required in order to achieve good numerical convergence is an approximation of c_n and c_t that falls within a few orders of magnitude of the optimal selection. More details on mortar finite element formulations for contact mechanics can be found in Popp's Ph.D. thesis [23]. These equations, within a semi-smooth Newton solution strategy, guarantee local superlinear convergence of the Coulomb frictional problem, i.e. nodal states of stick, slip, and not in contact. For rigorous analyses of convergence, see [24, 25].

Finally, in this work, we add a strategy to stabilize the contact constraints in order to better preserve the energy of the system. Stabilization of the normal contact constraint may also be seen as adding a so-called "persistency" condition [22]. Such a condition entails the enforcement of normal contact constraint on the velocity level once it is established that a particular node is in contact. We rely on monitoring each node's weighted gap ($\tilde{g}_{n,j}$). If the node was also in contact at the last time step, Eqn. 6 is no longer used. Instead, the nonlinear complementarity condition for normal contact becomes:

$$C_j(\boldsymbol{u}, \boldsymbol{\lambda}) = \lambda_{n,j} - \max(0, \lambda_{n,j} - c_n \dot{\tilde{g}}_{n,j}) = 0, \quad c_n > 0, \tag{9}$$

where the weighted gap velocity, $\dot{\tilde{g}}_{n,j}$, is defined as:

$$\dot{\tilde{g}}_{n,j} = \int_{\gamma_c^{(1)}} \phi_j(\boldsymbol{\xi}) \dot{g}^h(\boldsymbol{\xi}) \mathrm{d}\gamma_c^{(1)}. \tag{10}$$

When using an implicit scheme, the gap velocity must undergo time discretization to ensure that no change in interpenetration occurs during the time step. This is achieved by introducing the Newmark-β scheme in the gap definition. Thus, as a function of the displacement variables, the weighted gap velocity must be computed based on the following nodal displacement rate variable vector:

$$\dot{\boldsymbol{u}}^{t+1} = \frac{\gamma}{\beta} \frac{\boldsymbol{u}^{t+1} - \boldsymbol{u}^t}{\Delta t} + \dot{\boldsymbol{u}}^t, \tag{11}$$

where $\boldsymbol{u}$ denotes the vector of nodal displacements, $(\dot{\ })$ denotes the time derivative of a quantity, the exponent refers to the time step, and γ and β are the traditional Newmark-β's numerical time integration parameters.

This strategy enables separation of the node, and if in contact, the Lagrange multiplier takes a value such that interpenetration does not change during the time step. Note that, when a node first comes into contact with the primary surface, a non-zero interpenetration that depends on the time step size may be generated. However, this interpenetration is typically negligible, since small time steps are required anyway to properly capture impacts.

The Jacobian of the contact constraints and their corresponding generalized forces acting on the displacement variables are computed by means of an automatic differentiation C++ library [26]. Its practical use in this work is summarized in Appendix A.

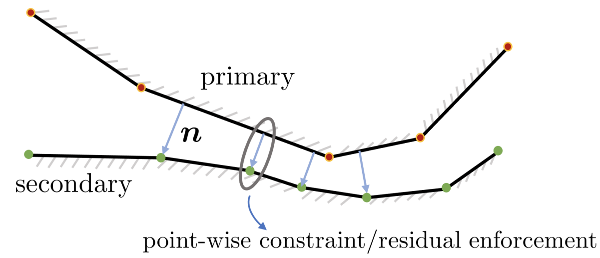

Fig. 2: SCHEME SHOWING THE SIMPLE GEOMETRY USED FOR NODE-TO-SEGMENT NORMAL CONTACT ENFORCEMENT.

4 NODE-TO-SEGMENT MECHANICAL CONTACT

Unlike the enforcement of constraints presented in the previous section, the typical approach to contact constraint enforcement relies on NTS projections and corresponding residual computations. In essence, Eqn. 2 is enforced through the simple projection of nodes onto one of the contacting surfaces. MOOSE uses a kinematic contact approach in which the pointwise normal gap is iteratively reduced using a penalty parameter. The contact residual is computed as follows:

$$\boldsymbol{f}_c = \sum_i \boldsymbol{n}_j \boldsymbol{n}_j^T k_p g_{n,j}, \tag{12}$$

where $\boldsymbol{f}_c$ is the converged normal contact force, $\boldsymbol{n}_j$ denotes the normal vector at a node j, $g_{n,j}$ is a pointwise gap, k_p is a "penalty" parameter, and i denotes the iteration number. The contact constraint force in this approach is iteratively updated until the gap is zero (i.e., tolerance is satisfied). As such, k_p is a penalty parameter that does not affect the quality of kinematic contact enforcement, but can affect convergence behavior. The summation in Eqn. 12 stops when the number of iterations i satisfies the contact constraint. The geometry of this type of NTS enforcement is greatly simplified compared to the mortar approach presented above, as is observed in Fig. 2.

As the lack of variational consistency in NTS formulations usually manifests itself in noisy contact results and convergence problems, authors and developers have resorted to heuristic geometry smoothing. One example of this alleviating approach is to perform some kind of interpolation of the discrete normal vectors involved in contact/residual enforcement. To this effect, MOOSE features the ability to smooth out normal vectors within a certain distance from the edge of the finite element face. That is, by choosing a normalized distance, the code eliminates any sudden changes in geometry as contact moves from one finite element side to the next.

5 NUMERICAL RESULTS

This section presents 2-D numerical results from using both an NTS approach and an STS approach based on a mortar enforcement. The presented simulations were all performed using first-order Lagrange finite elements and employing Newton's method to solve the system of equations.

5.1 Stabilization of contact constraints

Under plane strain conditions, we consider a 2-D problem in which a block is kinematically driven in and out of contact against a flexible, but much stiffer, substrate. The block dimensions are 1 m by 1 m. Its constitutive behavior is governed by isotropic elasticity with incremental finite strain, thus drawing on the multiplicative decomposition of the deformation gradient [19]. The block's Young's modulus is 1 MPa and its Poisson's ratio is 0.3. The upper boundary of this block is driven kinematically via the cosine function $\cos(\frac{2\pi}{4}t)$, where t is time. The bottom side of the substrate is fixed in both the x and y directions, its Young's modulus is 100 MPa, and the Poisson's ratio is selected to be 0.3. The density is assumed to be $7750\,\frac{\mathrm{kg}}{\mathrm{m}^3}$. Stiffness Rayleigh damping is added to both domains at 10%. Contact interaction is assumed to be frictionless.

The numerical integrator used is Newmark-β with parameters $\gamma = 0.5$ and $\beta = 0.25$. The time step is fixed to 0.025 s.

In this section, we employ the persistency condition in Eqn. 9 to stabilize the mortar contact constraints (i.e. "stabilized" mortar), whereas the NTS approach is used without attempting dynamic stabilization. The mortar approach without stabilization is also discussed (i.e. "static" mortar). The setup is run for 8 s. For the chosen material properties, the

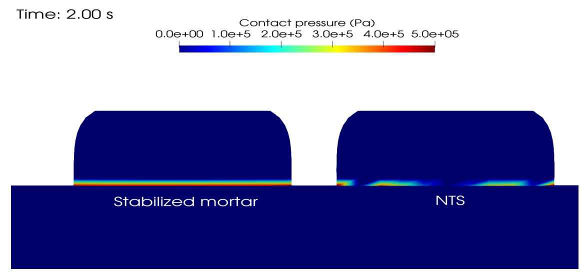

Fig. 3: SNAPSHOT OF THE SIMULATION, DEPICTING THE DISTRIBUTION OF NORMAL CONTACT PRESSURE. THE NODE-TO-SEGMENT APPROACH WITHOUT FURTHER STABILIZATION SHOWS ARTIFICIAL CHATTER ON THE CONTACT INTERFACE.

lack of stabilization in the NTS results causes chatter in contact pressure evolution. In other words, the contact formulation does not preserve the correct evolution of system energies. This behavior can be readily observed in Fig. 3, where the two separate simulations (one using a stabilized mortar approach and the other an NTS approach), are shown side by side at a time in which deformation of the block, which has an initially square section, is significant. There, the contact pressure computed at the interface shows an irregular pattern when NTS enforcement is used.

The elastic and kinetic energies of the entire 2-D system are plotted in Figs. 4 and 5, respective. Three contact formulations are employed: Static mortar, stabilized mortar, and NTS without stabilization. When using the NTS approach without stabilization, both the total kinetic and elastic energies show erratic behavior upon the block coming into contact with the substrate, which is shown with light blue background. The NTS simulation terminates at about 5.5s, at which time it demands smaller time steps. Similar behavior is shown by unstabilized mortar, which finishes the simulation with shifted kinetic energy. In fact, good agreement between these three approaches only exists when the block and substrate are not in contact and material damping had the time to remove the numerical artifacts. By taking a close look at Fig. 5, one can observe that, at the contact interface, the instabilities generated by the NTS and the static mortar approaches cause an increase in the system's kinetic energy and thus significantly affect the deformation. The poor results generated by the kinematically enforced NTS contact formulation are

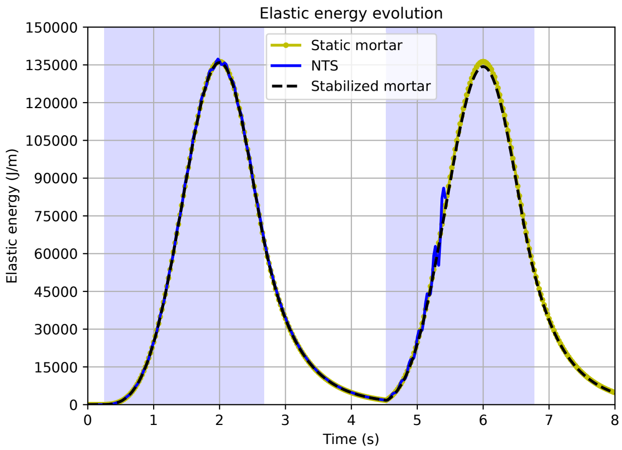

Fig. 4: ELASTIC ENERGY OF THE ENTIRE SYSTEM DURING THE SIMULATION. TIME SPANS WITH CONTACT ARE SHADED.

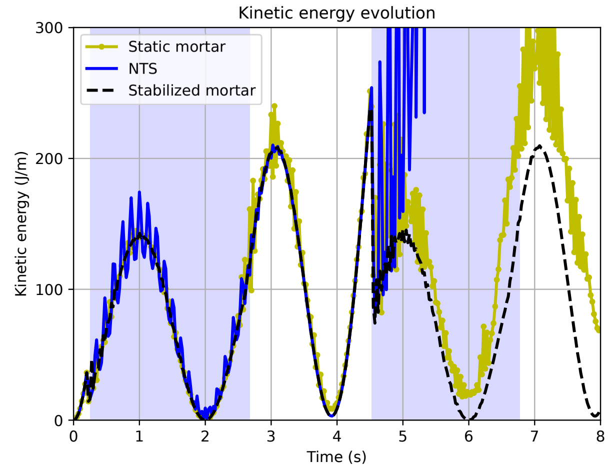

Fig. 5: KINETIC ENERGY OF THE ENTIRE SYSTEM DURING THE SIMULATION. UNDER THE NTS AND STATIC MORTAR APPROACHES, THE KINETIC ENERGY INCREASES DUE TO CONTACT INTERFACE INSTABILITIES (PARTIALLY TRUNCATED). TIME SPANS WITH CONTACT ARE SHADED.

also accompanied by struggling solver behavior, as shown in Fig. 6, where the cumulative nonlinear iteration count curve changes its slope when the bodies come into and remain in contact under the NTS formulation (note that contact starts at 0.2 and 4.52 s).

The behavior shown in this section is representative of the practical behavior of the formulations under comparison; however, the instabilities introduced by NTS and unstabilized mortar depend on the material properties, time step size, and other formulation parameters. For example, instabilities may be reduced with a selection of a smaller time step size. In addition, different choices of material stiffness will potentially lead to failure to complete the simulation, due to the artificial energy introduced on the contact interface. Regardless, these instabilities will still be present in the numerical results. In fact, as shown by this example, without stabilization, a reasonable selection of the time step size leads to severely compromising the viability and energy conservation of an implicit dynamic simulation.

5.2 Consistent discretization results in a dynamic problem

In this section, we select a problem with curved surfaces and large deformation. This problem setup is usually referred to in the literature as the "ironing" problem. The setup is simple: a semicircular tool is pushed into a substrate or block and then forced to slide laterally via Dirichlet boundary conditions. The lateral motion takes place while mechanical deformation in the blocks is significant. A drawing with the main model's dimensions is depicted in Fig. 7.

Both materials are assumed to be linear elastic, and strain increments are computed in a manner that accounts for finite strain kinematics. The semicircular tool and the substrate are assumed to have the same material parameters: namely, their Young's modulus and Poisson's ratio are 6896 and 0.32, respectively. Density, ρ, is 0.1, and the time step increment is selected to be 0.01 s. Stiffness Rayleigh damping for both blocks is assumed to be 0.5%. The selected degree of material stiffness causes both the tool and substrate to undergo significant deformation. The bottom of the substrate is fully fixed, and the top of the tool is driven in the x and y directions by the following functions: $u_x = t$ and, if $t > 2$, $u_y = -1.0$; otherwise, $u_y = -t/2.0$, where u_x and u_y denote displacement in the x and y directions with respect to the reference configuration, and t refers to simulation time. These functions force the tool to indent into the material while also moving horizontally during the first two seconds, then the semicircular tool continues to move laterally with fixed

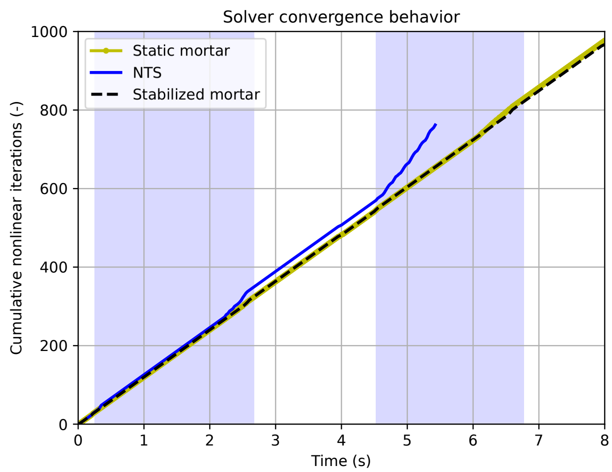

Fig. 6: CUMULATIVE NONLINEAR ITERATIONS REQUIRED TO SOLVE THE PROBLEM. WHEN THE BLOCK IS IN CONTACT WITH THE SUBSTRATE, THE NTS FORMULATION (SOLID BLUE LINE) MUST INCREASE THE NUMBER OF NONLINEAR ITERATIONS TO SOLVE THE PROBLEM. TIME SPANS WITH CONTACT ARE SHADED.

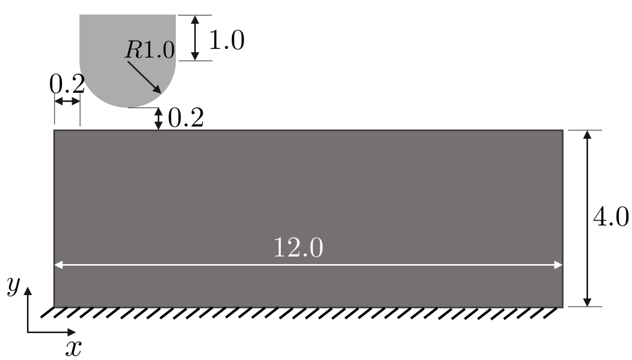

Fig. 7: SCHEMA WITH THE DIMENSIONS OF THE 2-D IRONING PROBLEM.

indentation displacement. The extent of mechanical deformation can be observed in Fig. 8.

This setup is simulated through three approaches: NTS (no geometry smoothing), NTS with maximum normal vector smoothing, and mortar mechanical contact. The frictionless problem yields the contact pressure evolution of a node on the semicircular tool, and this evolution is plotted in Fig. 9.

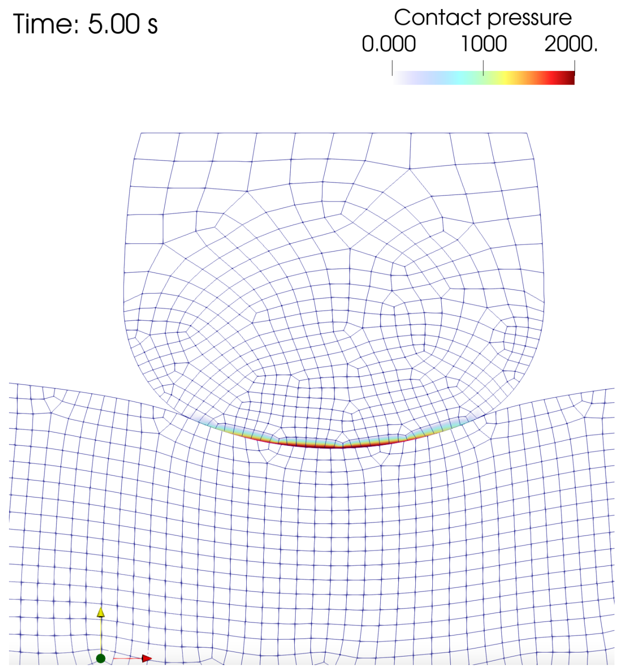

Fig. 8: MESH AND CONTACT PRESSURE DISTRIBUTION AT ONE INSTANT OF THE SIMULATION WITH STABILIZED DUAL MORTAR CONTACT CONSTRAINTS.

The NTS formulation cannot solve the problem once the tool has been pushed into the substrate to the level of maximum displacement: the simulation becomes unstable after generating a contact pressure frequency that markedly corresponds to $\approx 16.6\,\text{Hz}$, which is the nodal element-passage frequency. Spatially smoothing the nodal normal vector as much as possible allows the simulation to be completed (NTS with normal smoothing). Finally, the mortar contact formulation, without any ad hoc geometry smoothing, can complete the simulation in a robust fashion. Results show that smoothing the normal vector for NTS still generates artificial oscillations of significant amplitude. The amplitude of these oscillations can certainly be too large when contact interface dynamics are of relevance (see Fig. 10 for a close-up). Note that, unlike what happens in the bouncing block problem (see Fig. 3), the NTS simulation does not destabilize over time in the ironing problem, nor are the resulting numerical frequencies related to the system's frequencies. In other words, the phenomenon presented in this section is independent of the issue of constraint stabilization, but is related to the variational consistency of the contact dynamic formula-

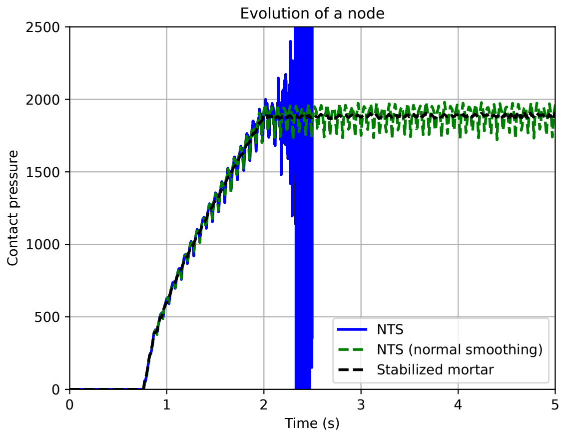

Fig. 9: EVOLUTION OF NODAL CONTACT PRESSURE FOR THE IRONING PROBLEM. NTS, NTS WITH GEOMETRY SMOOTHING, AND STABILIZED MORTAR ARE PLOTTED.

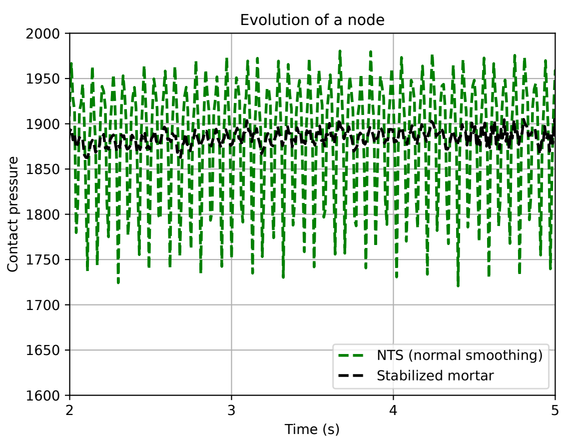

Fig. 10: CLOSE-UP OF THE EVOLUTION OF NODAL CONTACT PRESSURE FOR THE IRONING PROBLEM.

tion.

Using the same numerical parameters, we ran the ironing problems with Coulomb friction, assuming a coefficient of friction $\mu = 0.25$. As a result of adding the friction, the semicircular tool became sheared (see Fig. 11). The normal pressure evolution at a single node on the contact interface is plotted in Fig. 12, which shows that the same undesirable oscillation occurs when running our frictional NTS con-

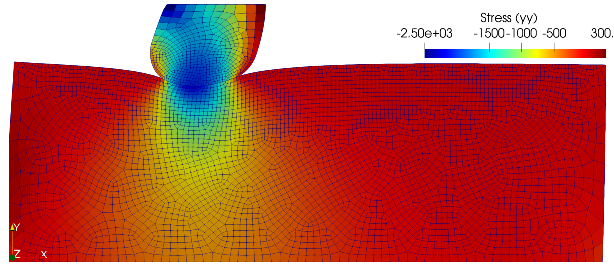

Fig. 11: NORMAL STRESS DISTRIBUTION (σ_y) OF THE BLOCK AND TOOL WHEN THE SIMULATION IS RUN WITH A FRICTION COEFFICIENT OF 0.25 (MORTAR). THE TOOL IS SHEARED DUE TO THE FRICTIONALLY SATURATED (SLIP STATE) CONTACT INTERFACE HAVING GENERATED A NET FORCE THAT IS IN OPPOSITION TO THE TOOL'S MOTION.

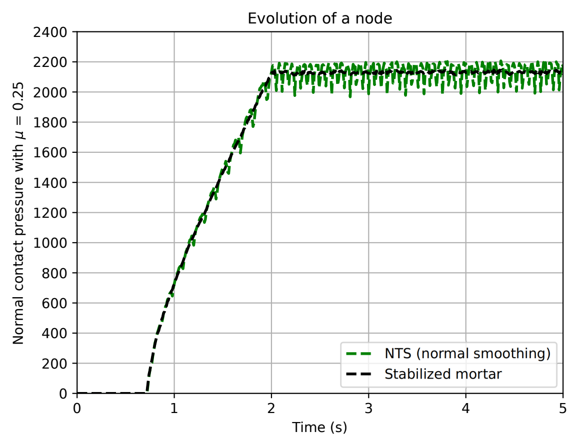

Fig. 12: NORMAL CONTACT PRESSURE EVOLUTION OF A NODE ON THE CONTACT INTERFACE, AS DETERMINED USING BOTH NTS WITH NORMAL GEOMETRY SMOOTHING AND STABILIZED MORTAR.

tact formulation. The normal contact pressure is a key input to the frictional components of the contact force (see Eqn. 4) and thus has direct implications on the time evolution of stresses and friction-derived quantities (e.g., frictional energy or wear equations).

6 DISCUSSION

This manuscript covers the application and analysis of known contact mechanics formulations in the context of implicit solutions for dynamic finite element formulations. Variationally consistent formulations such as the mortar method can pass the contact patch test (the counterpart to the finite element patch test) and yield better numerical convergence compared to NTS approaches. Though these features of mortar contact are known, the benefits of a consistent contact mechanics formulation in dynamic simulations are hardly touched upon in the literature. Here, we discuss a couple of eminently dynamic phenomena that contribute to the accuracy of contact interface dynamic modeling.

First, the importance of properly stabilizing contact constraints is highlighted via the application of mortar- and NTS-based contact formulations. While constraints are stabilized for the mortar formulation, they are not for the NTS formulations presented herein (similar energy artifacts are observed if the mortar constraints are not stabilized). This effect is covered in the literature, with the "persistency" condition being employed to enforce proper energy conservation. Despite this aspect being known (see, e.g., [27]), this formulation feature is often missing in dynamic implementations. In addition, when using a penalty approach, typical multibody formulations employ the approximation $f_c = k\delta^n + c\dot{\delta}$, where δ represents the interpenetration, n is a formulation-dependent exponent, k denotes a stiffness parameter, and c denotes a damping coefficient. While this approach can effectively mask the lack of contact constraint stabilization via its damping term and a permanent interpenetration while in contact, it also adds an artificial dynamical subsystem on the contact interface. This added dynamics on the interface is not at all physical unless Hertz or Hertz-like theories happen to apply. For this reason, special care is required to not affect the dynamic response of the simulated systems—particularly when high frequencies are of interest (e.g., corrugation in railroad systems, tire-rough surface interaction, and machining).

Second, we highlight a phenomenon of variational consistency that occurs in contact dynamics formulations but has not received much attention in the related literature: namely, the numerical artifacts created by the relative sliding of finite element meshes. Mortar segments in the lower-dimensional domains are created, and the corresponding contact constraints enforced, every time the system requires evaluation. The size of the segments changes as two contacting surfaces move relative to each other, thus providing a piece-wise smoothing contribution to the constraints and forces. The smoothness of the discretized contact enforcement when using mortar constraints enables seamless evolution of contact forces, as finite elements with different normal vectors move tangentially. This effect is relevant to dynamics, as the finite element discretization generates a numerical force that excites the system. The mortar results are then compared with a typical NTS implementation—as implemented in MOOSE. Results show that the NTS approach fails to provide the required smoothness in numerical results, even with smoothing of the normal vectors. While this effect is not restricted to dynamic simulations (see [28] for similar ironing problem results from a quasi-static simulation), this undesirable aspect of the NTS approach can indeed excite fundamental system frequencies that render the computational modeling effort unusable.

Instabilities in the solutions of contact interface problems have key consequences in the solutions of quasi-static contact mechanics problems. In the case of dynamics, inconsistencies in the contact dynamics simulations often affect the simulation at large and can prevent its completion. The present study suggests that use of variationally consistent contact mechanics approaches is strongly recommended when contact determines the dynamic evolution of a system. The numerical artifacts generated by inconsistent contact formulations have additional relevance in regard to friction-originated phenomena in which, for example, wear can drive the evolution of a system via normal and frictional contact forces.

ACKNOWLEDGEMENTS

This work is supported by the INL Laboratory Directed Research & Development (LDRD) Program under DOE Idaho Operations Office contract no. DE-AC07-05ID14517. Accordingly, the U.S. Government retains a non-exclusive, royalty-free license to publish or reproduce the published form of this contribution, or allow others to do so, for U.S. Government purposes.

APPENDIX A: AUTOMATIC DIFFERENTIATION

The system of nonlinear algebraic equations resulting from finite element discretization is solved via Newton's method. The contribution of the mortar constraints to the system's Jacobian matrix is computed using the MOOSE automatic differentiation (AD) system. The AD library enables the repeated application of the chain rule with a forward mode [26].

This library is integrated via an application programming interface in C++ programming via the employment of AD objects, which contain a residual's, possibly intermediate, value and its corresponding derivatives with respect to each of the primal, displacement and Lagrange multiplier variables. Displacement variables involved in a nodal constraint encompass neighboring finite elements within the secondary domain and the nodal displacement variables involved in the projections from the primary surface used to build the lower-dimensional domain on the contact interface. As an example, computation of the zero-penetration constraint begins with adding quadrature-point gap derivative information (which is accessed via the _qp quadrature point index), as shown in Listing 1. Each automatic differentiation object, such as ADRealVectorValue, has a derivative container and can access the derivative entries corresponding to each degree of freedom via the method derivatives(). As such, Gaussian numerical integration on the gap value on the lower dimensional domain (_qp_gap) takes place while propagating the derivative information. The gap vector _gap_vec, the Jacobian of the mortar segment element mapping times the integration rule weights _JxW_msm, and a possible coordinate transformation _coord are used in determining the integrand of Eqn 7. After looping through the mortar segment mesh and assembling the weighted gaps, these are compared against the normal contact pressure at a node j, represented by $\lambda_{n,j}$, in a nonlinear complementarity problem (NCP) representation of the zero-penetration portion of Listing 2. The application programming interface shown in Listing 2 shows the ease of use in the definition of residuals and Jacobians when employing automatic differentiation objects, thereby removing the need for lengthy Jacobian derivations, either to employ a Newton procedure or to build a preconditioner in Jacobian-free schemes. weighted_gap is the numerically integrated normal gap at a node, c denotes the c_n coefficient –which can be normalized with the mortar segment size in order to aid in its selection. The variable number _var->number() is used to obtain the degree of freedom number together with the nonlinear system object of this problem, i.e _sys.number(). When needed, derivative values can be added to the array by employing the function Moose::derivInsert, which is used to signal the trivial dependency of a Lagrange multiplier value with itself (e.g. lm_value). processDerivatives(...) and cacheResidual(...) allow the assembly system to build the Jacobian with automatically obtained derivatives and to populate the constraint residual, respectively. This construction of the NCP representation by using automatic differentiation is shown in Listing 2. In a way similar to that presented in this Appendix, the frictional contact constraints and their residuals leverage AD C++ objects.

Using automatic differentiation to compute contributions to the system's Jacobian limits inaccuracies and leads to a more efficient nonlinear solve in terms of nonlinear iteration count. However, because derivative information with respect to the displacements is not currently available for the normal and tangent vectors, the computed Jacobian is imperfect and a Jacobian-free method may have to be used to approximate the action of the Jacobian on a vector, using finite differencing of the residual vector, for problems in which this approximation is not good enough. Future work will examine extending the automatic differentiation system to the positions of mesh nodes, and from there to fundamental mortar mesh quantities such as normal and tangent vectors. This would enable perfect computation of the Jacobian.

```
ADRealVectorValue gap_vec = _phys_points_primary[_qp]
    -
                            _phys_points_secondary[_qp
    ];

gap_vec(0).derivatives() =
    _primary_disp_x[_qp].derivatives() -
    _secondary_disp_x[_qp].derivatives();
gap_vec(1).derivatives() =
    _primary_disp_y[_qp].derivatives() -
    _secondary_disp_y[_qp].derivatives();
if (_has_disp_z)
  gap_vec(2).derivatives() =
      (*_primary_disp_z)[_qp].derivatives() -
      (*_secondary_disp_z)[_qp].derivatives();

if (_interpolate_normals)
  _qp_gap = gap_vec *
            (_normals[_qp] * _JxW_msm[_qp] * _coord[
    _qp]);
else
  _qp_gap_nodal = gap_vec * (_JxW_msm[_qp] * _coord[
    _qp]);
```

Listing 1: GAP DERIVATIVE SEEDING

```
const auto & weighted_gap = *_weighted_gap_ptr;
// Optionally normalize with the mortar segment volume
const Real c =
    _normalize_c ? _c / *_normalization_ptr : _c;
```

```

// Get the degree of freedom index for the Lagrange
// Multiplier (LM) variable
const auto dof_index =
    dof->dof_number(_sys.number(), _var->number(), 0);
// Query the solution vector for the LM value at our
    dof
// index
ADReal lm_value = (*_sys.currentSolution())(dof_index)
    ;
// Seed the LM derivative for the automatic
// differentiation representation
Moose::derivInsert(lm_value.derivatives(), dof_index,
    1.);

// NCP representation of the zero-penetration
    constraint.
// Through operator overloading of std::min, the
    result of
// std::min is an automatic differentiation type,
    ADReal
const ADReal dof_residual =
    std::min(lm_value, weighted_gap * c);

// Process the constraint into either the system
    Jacobian
// matrix or system residual vector
if (_subproblem.currentlyComputingJacobian())
  _assembly.processDerivatives(
      dof_residual, dof_index, _matrix_tags);
else
  _assembly.cacheResidual(
      dof_index, dof_residual.value(), _vector_tags);
```

Listing 2: ZERO-PENETRATION CONSTRAINT FORMATION

REFERENCES

[1] Laursen, T. A., 2003, Computational Contact and Impact Mechanics Springer Berlin Heidelberg, Berlin, Heidelberg.

[2] Wriggers, P., 2006, Computational Contact Mechanics Springer Berlin Heidelberg, Berlin, Heidelberg.

[3] Wohlmuth, B. I., 2000, “A mortar finite element method using dual spaces for the Lagrange multiplier,” SIAM journal on numerical analysis, 38(3), pp. 989–1012.

[4] Wohlmuth, B., 2011, “Variationally consistent discretization schemes and numerical algorithms for contact problems,” Acta Numerica, 20, pp. 569–734.

[5] Popp, A., and Wall, W., 2014, “Dual mortar methods for computational contact mechanics–overview and recent developments,” GAMM-Mitteilungen, 37(1), pp. 66–84.

[6] Seitz, A., Wall, W. A., and Popp, A., 2019, “Nitsche’s method for finite deformation thermomechanical contact problems,” Computational Mechanics, 63(6), pp. 1091–1110.

[7] Drouet, G., and Hild, P., 2017, “An accurate local average contact method for nonmatching meshes,” Numerische Mathematik, 136(2), pp. 467–502.

[8] Abbas, M., Drouet, G., and Hild, P., 2018, “The local average contact (LAC) method,” Computer Methods in Applied Mechanics and Engineering, 339, pp. 488–513.

[9] Yang, B., Laursen, T. A., and Meng, X., 2005, “Two dimensional mortar contact methods for large deformation frictional sliding,” International journal for numerical methods in engineering, 62(9), pp. 1183–1225.

[10] Puso, M. A., Laursen, T., and Solberg, J., 2008, “A segment-to-segment mortar contact method for quadratic elements and large deformations,” Computer Methods in Applied Mechanics and Engineering, 197(6), pp. 555–566.

[11] Papadopoulos, P., and Taylor, R. L., 1992, “A mixed formulation for the finite element solution of contact problems,” Computer Methods in Applied Mechanics and Engineering, 94(3), pp. 373–389.

[12] Seitz, A., Farah, P., Kremheller, J., Wohlmuth, B. I., Wall, W. A., and Popp, A., 2016, “Isogeometric dual mortar methods for computational contact mechanics,” Computer Methods in Applied Mechanics and Engineering, 301, pp. 259–280.

[13] Shabana, A., 2020, Dynamics of multibody systems Cambridge university press.

[14] Permann, C. J., Gaston, D. R., Andrš, D., Carlsen, R. W., Kong, F., Lindsay, A. D., Miller, J. M., Peterson, J. W., Slaughter, A. E., Stogner, R. H., et al., 2020, “MOOSE: Enabling massively parallel multiphysics simulation,” SoftwareX, 11, p. 100430.

[15] Gitterle, M., Popp, A., Gee, M. W., and Wall, W. A., 2010, “Finite deformation frictional mortar contact using a semi-smooth newton method with consistent linearization,” International Journal for Numerical Methods in Engineering, 84(5), pp. 543–571.

[16] Tal, Y., and Hager, B. H., 2018, “Dynamic mortar finite element method for modeling of shear rupture on frictional rough surfaces,” Computational Mechanics, 61(6), pp. 699–716.

[17] Heinstein, M. W., and Laursen, T. A., 1999, “An algorithm for the matrix-free solution of quasistatic frictional contact problems,” International journal for numerical methods in engineering, 44(9), pp. 1205–1226.

[18] Puso, M., and Solberg, J., 2020, “A dual pass

mortar approach for unbiased constraints and self-contact," Computer Methods in Applied Mechanics and Engineering, 367, p. 113092.

[19] Rashid, M., 1993, "Incremental kinematics for finite element applications," International Journal for Numerical Methods in Engineering, 36(23), pp. 3937–3956.

[20] Carvalho, R. P., Carneiro, A., Pires, F., and Popp, A., 2022, "An efficient algorithm for rigid/deformable contact interaction based on the dual mortar method," Computational Mechanics, pp. 1–25.

[21] Knoll, D., and Keyes, D., 2004, "Jacobian-free newton–krylov methods: a survey of approaches and applications," Journal of Computational Physics, 193(2), pp. 357–397.

[22] Hüeber, S., 2008, "Discretization techniques and efficient algorithms for contact problems," PhD Thesis, University of Stuttgart.

[23] Popp, A., 2012, "Mortar methods for computational contact mechanics and general interface problems," PhD thesis, Technische Universität München, 6.

[24] Hüeber, S., Stadler, G., and Wohlmuth, B. I., 2008, "A primal-dual active set algorithm for three-dimensional contact problems with coulomb friction," SIAM Journal on scientific computing, 30(2), pp. 572–596.

[25] Hintermüller, M., Ito, K., and Kunisch, K., 2002, "The primal-dual active set strategy as a semismooth newton method," SIAM Journal on Optimization, 13(3), pp. 865–888.

[26] Lindsay, A., Stogner, R., Gaston, D., Schwen, D., Matthews, C., Jiang, W., Aagesen, L. K., Carlsen, R., Kong, F., Slaughter, A., Permann, C., and Martineau, R., 2021, "Automatic differentiation in MetaPhysicL and its applications in MOOSE," Nuclear Technology, Feb., pp. 1–18.

[27] Laursen, T., and Love, G., 2002, "Improved implicit integrators for transient impact problems—geometric admissibility within the conserving framework," International Journal for Numerical Methods in Engineering, 53(2), pp. 245–274.

[28] Yushu, D., Martin Recuero, A., Schwen, D., Lindsay, A. D., and Spencer, B. W., 2021, M3 milestone: Advanced contact 2021 Tech. rep., Idaho National Lab.(INL), Idaho Falls, ID (United States).